1-1-2014

In-situ neutron diffraction of LaCoO3 perovskite under uniaxial compression. II. Elastic properties

Mykola Lugovy
University of Central Florida

Amjad Aman
University of Central Florida

Yan Chen
University of Central Florida

Nina Orlovskaya
University of Central Florida

Jakob Kuebler

In-situ neutron diffraction of $LaCoO_3$ perovskite under uniaxial compression. II. Elastic properties

Cite as: J. Appl. Phys. **116**, 013504 (2014); https://doi.org/10.1063/1.4884336
Submitted: 15 January 2014 . Accepted: 09 June 2014 . Published Online: 01 July 2014

Mykola Lugovy, Amjad Aman, Yan Chen, Nina Orlovskaya, Jakob Kuebler, Thomas Graule, Michael J. Reece, Dong Ma, Alexandru D. Stoica, and Ke An

In-situ neutron diffraction of $LaCoO_3$ perovskite under uniaxial compression. II. Elastic properties

Mykola Lugovy,[1,2] Amjad Aman,[1] Yan Chen,[1,3] Nina Orlovskaya,[1,a)] Jakob Kuebler,[4] Thomas Graule,[4] Michael J. Reece,[5] Dong Ma,[3] Alexandru D. Stoica,[3] and Ke An[3]
[1]*Department of Mechanical and Aerospace Engineering, University of Central Florida, Orlando, Florida 32816, USA*
[2]*Institute for Problems of Materials Science, Kiev 03142, Ukraine*
[3]*Chemical and Engineering Materials Division, Neutron Sciences Directorate, Oak Ridge National Laboratory, Oak Ridge, Tennessee 37831, USA*
[4]*Empa, Swiss Federal Laboratories for Materials Science and Technology, Laboratory for High Performance Ceramics, Ueberlandstrasse 129, 8600 Duebendorf, Switzerland*
[5]*The School of Engineering and Materials Science, Queen Mary, University of London, London E1 4NS, United Kingdom*

(Received 15 January 2014; accepted 9 June 2014; published online 1 July 2014)

Calculations of elastic constants and development of elastic anisotropy under uniaxial compression in originally isotropic polycrystalline $LaCoO_3$ perovskite are reported. The lattice strains in individual (*hkl*) planes as well as average lattice strain were determined both for planes oriented perpendicular and parallel to the loading direction using in-situ neutron diffraction. Utilizing average lattice strains as well as lattice strains along the *a* and *c* crystallographic directions, an attempt was made to determine Poisson's ratio of $LaCoO_3$, which was then compared with that measured using an impulse excitation technique. The elastic constants were calculated and Young's moduli of $LaCoO_3$ single crystal in different crystallographic directions were estimated. © *2014 AIP Publishing LLC*. [http://dx.doi.org/10.1063/1.4884336]

I. INTRODUCTION

The mechanical properties of $LaCoO_3$ ceramics have been extensively investigated in the past decade and ferroelastic deformation along with time dependent room temperature creep has been reported.[1–4] However, only a few publications have reported the elastic properties of $LaCoO_3$, where Young's and bulk moduli were investigated as a function of temperature and stress.[5,6] The results reported showed that the Young's modulus, measured from the slope of a stress-strain deformation curve, was equal to 76 GPa at the very beginning of uniaxial compression, but increased by almost 2.5 times to 194 GPa when measured at the beginning of unloading from a compressive stress of 900 MPa.[7] The texture and formation of preferred domain orientation during uniaxial compression were studied and it was shown that at high applied stress, there was a significant growth of ferroelastic domains with preferred crystallographic orientations at the expense of other domain orientations. Upon unloading in the first cycle, partial recovery/reappearance of other crystallographic domains was observed. However, the preferred domain orientation and the texture formed in $LaCoO_3$ remained after the load was removed. This domain switching phenomenon was responsible for the hysteresis during a loading/unloading cycle as well as for the appearance of irreversible strain upon unloading since not all domains/twins were recovered to their initial state before deformation. Elastic anisotropy was introduced during such uniaxial loading, therefore the elastic properties of the polycrystalline $LaCoO_3$ are also expected to change. As texture formation is inevitably connected to the growth of preferred crystallographic orientation and an increase in the volume fraction of certain domains, if the elastic constants are known then it would be possible to estimate the anisotropy and calculate the elastic properties of polycrystalline $LaCoO_3$ in different crystallographic directions. Using neutron diffraction, the lattice parameters can be calculated as a function of applied compressive stress and other crystal structure analysis can be performed. This makes the possibility to evaluate the elastic constants and to calculate the elastic properties of pure $LaCoO_3$. Here, we report our results of the aforementioned evaluations along with an estimation of the elastic anisotropy present in $LaCoO_3$.

II. EXPERIMENTAL AND METHODOLOGY

The properties of the polycrystalline $LaCoO_3$ and the conditions for the *in-situ* uniaxial compression neutron diffraction experiments have been described in our previous work.[5,7,8] The properties of the $LaCoO_3$ ceramics are listed

TABLE I. Bulk properties of $LaCoO_3$ polycrystalline perovskite.

Property	Value
Porosity, %	4
Average grain size, μm	2–5
Young's modulus, GPa	76
Shear modulus, GPa	28.7
Poisson ratio	0.32

[a)]Author to whom correspondence should be addressed. Electronic mail: Nina.Orlovskaya@ucf.edu

in Table I. Most of the calculations performed in the current paper were done utilizing the neutron diffraction results obtained from Ref. 7. The present evaluation used the loading data during the neutron diffraction. Some of the data used are from a separate study in which tests were performed using uniaxial compression of $LaCoO_3$ to verify the change of Young's modulus as a function of applied stress when no neutron radiation was present.[9] In the current study, to determine Young's modulus of $LaCoO_3$ using the slope of the unloading stress-strain deformation plots, the following uniaxial compression experiments were performed. The uniaxial loading/unloading cycling was done using cylindrical samples of 6 mm in diameter and 12 mm height, in a servohydraulic testing machine (Instron 8511) with a 20 kN load cell under load control with a loading rate of 180 MPa/min. The compressive stress with a cyclic stress step of 33 MPa was applied parallel to the axis of the cylindrical samples. The axial strain was measured using three strain gauges mounted on the surface of each sample. The total strain was determined by averaging the signals from the three strain gauges.

In addition to uniaxial compression, the impulse excitation technique was used to measure Young's and shear moduli of $LaCoO_3$. Young's modulus E_0 and the shear modulus G_0 of the material were measured at room temperature on two samples, each. The samples had a length of ~36 mm, a width of ~8.0 mm, and a height of ~1.5 mm. For each sample, the density was calculated from its size and weight. The E_0 and G_0 measurements were performed in accordance to standard EN 843-2, Method D: Impulse excitation using a Grindo-Sonic Mk5 Industrial (Lemmens, Belgium) with a homemade sample holder.[10] Using E_0 and G_0, Poisson's ratios ν were calculate by using the equation $\nu = \frac{E_0}{2G_0} - 1$.

For the collected neutron diffraction patterns, the classification of the (hkl) peaks and their intensities in $LaCoO_3$ were adopted from Ref. 11, where the domains' volume fractions as a function of applied stress were analyzed with respect to the angle between the normal to the individual (hkl) diffraction plane and the c hexagonal axis. The peak's classification was adopted to differentiate peaks with diffraction planes with angles less than 45°, and the peaks with (hkl) planes with angles higher than 45°.[11]

For each (hkl) plane, the lattice strains $\varepsilon_{hkl}^{D1}(\sigma^{(i)})$ and $\varepsilon_{hkl}^{D2}(\sigma^{(i)})$ are calculated as a function of applied compressive stress, where

$$\varepsilon_{hkl}^{D1}(\sigma^{(i)}) = \frac{d_{hkl}^{D1}(\sigma^{(i)}) - d_{hkl}^{D1}(\sigma^{(0)})}{d_{hkl}^{D1}(\sigma^{(0)})}, \quad (1)$$

$$\varepsilon_{hkl}^{D2}(\sigma^{(i)}) = \frac{d_{hkl}^{D2}(\sigma^{(i)}) - d_{hkl}^{D2}(\sigma^{(0)})}{d_{hkl}^{D2}(\sigma^{(0)})}, \quad (2)$$

where $d_{hkl}^{D1}(\sigma^{(i)})$ and $d_{hkl}^{D2}(\sigma^{(i)})$ are the spacings of the various (hkl) lattice planes measured by detectors 1 and 2 (parallel and perpendicular to the applied stress), respectively, and i indicates the corresponding applied stress $\sigma^{(i)}$ (or run).

For the calculations of the, a_i^{D1}, c_i^{D1}, a_i^{D2}, and c_i^{D2}, lattice parameters as a function of applied stress, the procedure used was as shown in the work by Daymond *et al.*[12] Six peaks, (006), (018), (208), (024), (202), and (220), were used for the calculations using their known $d_{hkl}^{D1}(\sigma^{(i)})$, $d_{hkl}^{D2}(\sigma^{(i)})$, and (hkl) Miller indices with a valid assumption that a_i^{D1}, c_i^{D1}, a_i^{D2}, and c_i^{D2} parameters are the same for all peaks under consideration (Table II). Taking this assumption into account, the a_i^{D1}, c_i^{D1}, a_i^{D2}, and c_i^{D2} lattice parameters can be determined by using the least squares method for the following expressions:

$$\sum_{hkl}\left[\frac{1}{(d_{hkl}^{D1}(\sigma^{(i)}))^2} - \frac{4}{3}\left(\frac{h^2+hk+k^2}{(a_i^{D1})^2}\right) - \frac{l^2}{(c_i^{D1})^2}\right]^2, \quad (3)$$

$$\sum_{hkl}\left[\frac{1}{(d_{hkl}^{D2}(\sigma^{(i)}))^2} - \frac{4}{3}\left(\frac{h^2+hk+k^2}{(a_i^{D2})^2}\right) - \frac{l^2}{(c_i^{D2})^2}\right]^2. \quad (4)$$

Since two detectors were used for the collection of diffraction patterns,[7] the a_i^{D1} and c_i^{D1} determined from reflections parallel to the applied stress direction were from the lattice planes under compression, and a_i^{D2} and c_i^{D2} determined from reflections perpendicular to the applied stress direction were collected from the lattice planes under tension. Once a_i^{D1}, c_i^{D1}, a_i^{D2}, and c_i^{D2} are determined both for tension and for compression, the average lattice strains $\varepsilon_{ave}^{D1}(\sigma^{(i)})$ and $\varepsilon_{ave}^{D2}(\sigma^{(i)})$ can be found by averaging the strains connected with a_i and c_i[12] by using the expressions

$$\varepsilon_{ave}^{D1}(\sigma^{(i)}) = \frac{2\varepsilon_a^{D1}(\sigma^{(i)}) + \varepsilon_c^{D1}(\sigma^{(i)})}{3}, \quad (5)$$

$$\varepsilon_{ave}^{D2}(\sigma^{(i)}) = \frac{2\varepsilon_a^{D2}(\sigma^{(i)}) + \varepsilon_c^{D2}(\sigma^{(i)})}{3}, \quad (6)$$

where

$$\varepsilon_a^{D1}(\sigma^{(i)}) = \frac{a_i^{D1} - a_0^{D1}}{a_0^{D1}}, \quad (7)$$

$$\varepsilon_c^{D1}(\sigma^{(i)}) = \frac{c_i^{D1} - c_0^{D1}}{c_0^{D1}}, \quad (8)$$

$$\varepsilon_a^{D2}(\sigma^{(i)}) = \frac{a_i^{D2} - a_0^{D2}}{a_0^{D2}}, \quad (9)$$

$$\varepsilon_c^{D2}(\sigma^{(i)}) = \frac{c_i^{D2} - c_0^{D2}}{c_0^{D2}}. \quad (10)$$

TABLE II. Assignment of (hkl) planes to their respective orientation angles between the normal to diffraction plane and the c-axis.

Diffraction plane	Angle (deg)
(006)	0
(018)	19.2
(208)	34.8
(024)	54.3
(202)	70.2
(220)	90

As it was shown in the work of Daymond,[13] $\varepsilon_{ave}^{D1}(\sigma^{(i)})$ coincides well with continuum elastic strain measured during macroscopic deformation, therefore the equation

$$\sigma^{(i)} = E_i \varepsilon_{ave}^{D1}(\sigma^{(i)}) \tag{11}$$

can be utilized to determine Young's modulus of the material under investigation

$$E_i = \sigma^{(i)} / \varepsilon_{ave}^{D1}(\sigma^{(i)}). \tag{12}$$

The straightforward route to determine Young's moduli in different crystallographic directions, which in turn would determine the anisotropy of the material, would utilize

$$\sigma_{hkl}^{(i)} = E_{hkl} \varepsilon_{hkl}^{D1}(\sigma^{(i)}), \tag{13}$$

where $\sigma_{hkl}^{(i)} = \sigma^{(i)} + \sigma_{hkl}^{m}$ is the average stress along loading direction in the domains with (hkl) planes oriented normal to the loading direction, E_{hkl} is Young's modulus measured in the direction normal to the (hkl) planes, and σ_{hkl}^{m} is the local misfit stress generated by the grain anisotropy.

However, Eq. (11) is not valid if instead of $\varepsilon_{ave}^{D1}(\sigma^{(i)})$, the $\varepsilon_{hkl}^{D1}(\sigma^{(i)})$ of individual crystallographic spacing of the grain is used. The reason that Eq. (11) is not valid, when individual $\varepsilon_{hkl}^{D1}(\sigma^{(i)})$ is used, is the presence of local misfit stress σ_{hkl}^{m}, generated by the grain anisotropy. Such misfit stress depends on grain morphology and its surrounding, the grain boundaries' properties, and the history of ferroelastic deformation the grain experienced during loading. Since σ_{hkl}^{m} is unknown and cannot be measured, the following approach was used in the present paper to determine Young's modulus of $LaCoO_3$ as a function of crystallographic orientation. If one considers that the macroscopic applied stress $\sigma^{(i)}$ is imposed on the bulk sample then the stress balance can be written as[13]

$$\sigma^{(i)} = \sum_{hkl} f_{hkl}^{(i)} \sigma_{hkl}^{(i)} = \sum_{hkl} f_{hkl}^{(i)} E_{hkl} \varepsilon_{hkl}^{D1}(\sigma^{(i)}), \tag{14}$$

where $f_{hkl}^{(i)}$ represents the fraction of grains in the volume with orientation (hkl) planes normal to the loading direction. The volume fraction of (hkl) domains normal to loading direction for a specific applied stress (run) i can be estimated by

$$f_{hkl}^{(i)} = \frac{I_{hkl}^{D1}(\sigma^{(i)}) / I_{hkl}^{D1}(\sigma^{(0)})}{\sum_{hkl} I_{hkl}^{D1}(\sigma^{(i)}) / I_{hkl}^{D1}(\sigma^{(0)})}, \tag{15}$$

where $I_{hkl}^{D1}(\sigma^{(i)})$ is the intensity of the (hkl) diffraction peak collected by detector 1 for the run i, $I_{hkl}^{D1}(\sigma^{(0)})$ is the intensity for the run 0. The stress balance (14) assumes the summation over all possible crystallographic directions. However, in practice, the main characteristic crystallographic orientations can be used to obtain good representation of stress balance.[13] As it was investigated in the work of Daymond,[13] the number of peaks used to calculate the average lattice strain can be as low as five, where results from use of five (hkl) peaks are indistinguishable compared with the results from using seven peaks or more. Therefore, only six peaks of $LaCoO_3$ were included for average lattice strain analysis. Thus, as $\sigma_{hkl}^{(i)}$ is unknown *a priori*, it will be replaced with $E_{hkl}\varepsilon_{hkl}^{D1}(\sigma^{(i)})$, as it was specified in (14).

For single crystal with $R\bar{3}c$ rhombohedral symmetry, the relationship between elastic stresses and strains can be expressed as[14]

$$\begin{bmatrix} \varepsilon_1 \\ \varepsilon_2 \\ \varepsilon_3 \\ \gamma_4 \\ \gamma_5 \\ \gamma_6 \end{bmatrix} = \begin{bmatrix} S_{11} & S_{12} & S_{13} & S_{14} & 0 & 0 \\ S_{12} & S_{11} & S_{13} & -S_{14} & 0 & 0 \\ S_{13} & S_{13} & S_{33} & 0 & 0 & 0 \\ S_{14} & -S_{14} & 0 & S_{44} & 0 & 0 \\ 0 & 0 & 0 & 0 & S_{44} & 2S_{14} \\ 0 & 0 & 0 & 0 & 2S_{14} & 2(S_{11}-S_{12}) \end{bmatrix} \begin{bmatrix} \sigma_1 \\ \sigma_2 \\ \sigma_3 \\ \sigma_4 \\ \sigma_5 \\ \sigma_6 \end{bmatrix}, \tag{16}$$

where S_{11}, S_{33}, S_{44}, S_{12}, S_{13}, S_{14} are the six independent elastic compliance coefficients, $\varepsilon_1 = \varepsilon_{11}$ $\varepsilon_2 = \varepsilon_{22}$ $\varepsilon_3 = \varepsilon_{33}$ $\gamma_4 = \varepsilon_{23} + \varepsilon_{32}$ $\gamma_5 = \varepsilon_{13} + \varepsilon_{31}$ $\gamma_6 = \varepsilon_{12} + \varepsilon_{21}$ are the strain components, $\sigma_1 = \sigma_{11}$ $\sigma_2 = \sigma_{22}$ $\sigma_3 = \sigma_{33}$ $\sigma_4 = \sigma_{23}$ $\sigma_5 = \sigma_{13}$ $\sigma_6 = \sigma_{12}$ are the stress components using Voigt notation. For rhombohedral $R\bar{3}c$ symmetry Young's modulus in the direction perpendicular to (hkl) plane, E_{hkl}, can be expressed by the following equation:[14]

$$E_{hkl} = \left\{ \frac{(h_n^2 + k_n^2 - h_n k_n)^2 (a_i^{D1})^4 S_{11} + l_n^4 (c_i^{D1})^4 S_{33} + (h_n^2 + k_n^2 - h_n k_n) l_n^2 (a_i^{D1} c_i^{D1})^2 (S_{44} + 2S_{13}) + 3\sqrt{3} h_n k_n l_n (h_n - k_n) (a_i^{D1})^3 c_i^{D1} S_{14}}{[(h_n^2 + k_n^2 - h_n k_n)(a_i^{D1})^2 + l_n^2 (c_i^{D1})^2]^2} \right\}^{-1}, \tag{17}$$

where S_{11}, S_{33}, S_{44}, S_{13}, and S_{14} are the elastic compliance coefficients, $h_n = \frac{2}{3(a_i^{D1})^2}(2h+k)$, $k_n = \frac{2}{3(a_i^{D1})^2}(h+2k)$, and $l_n = \frac{l}{(c_i^{D1})^2}$ are indices of the corresponding crystallographic directions in a hexagonal coordinate system.

Equation (17) has a dependence on lattice parameters. However, this represents a dependence of E_{hkl} on a/c ratio of lattice parameters, as one can see after simple transformations of Eq. (17). Besides, for directions parallel to the c-axis ($h_n = k_n = 0$) and for all directions perpendicular to c-axis ($l_n = 0$), there is no dependence of E_{hkl} on a, c, or a/c, which can be easily verified for Eq. (17). Additionally, in this case, the difference between a/c ratio at zero stress and at maximum applied stress (i.e. maximum variation) is less than

TABLE III. The estimated compliance coefficients for $LaCoO_3$ single crystal, determined from experimental data for polycrystalline material.

Compliance constants, GPa^{-1}				
S_{11}	S_{33}	S_{44}	S_{13}	S_{14}
2.9×10^{-2}	3.81×10^{-3}	7.69×10^{-3}	-1.59×10^{-3}	-9.6×10^{-3}

0.1%, thus a variation of parameter a/c with applied stress can be considered to be negligible. Therefore, no dependence of E_{hkl} on a, c, or a/c is found.

Using Eqs. (14) and (17), the compliance coefficients S_{11}, S_{33}, S_{44}, S_{13}, and S_{14} can be determined by finding the minimum of the following expression:

$$\sum_i \left[\sigma^{(i)} - \sum_{hkl} f_{hkl}^{(i)} E_{hkl} \varepsilon_{hkl}^{D1}(\sigma^{(i)})\right]^2. \quad (18)$$

In such a way, the macroscopic stress $\sum_{hkl} f_{hkl}^{(i)} E_{hkl} \varepsilon_{hkl}^{D1}(\sigma^{(i)})$ calculated from stress balance becomes the closest one to the applied stress $\sigma^{(i)}$.

The estimation of the upper and lower bounds of Young's modulus was also performed using the standard procedure.[15] In general, if the polycrystal is treated as a composite and domains with orientation (hkl) planes normal to the loading direction as separate phases, we can find upper and lower bounds for its Young's modulus using

$$E_i^{(V)} = \sum_{hkl} f_{hkl}^{(i)} E_{hkl} \quad (19)$$

and

$$E_i^{(R)} = \left[\sum_{hkl} (f_{hkl}^{(i)}/E_{hkl})\right]^{-1}. \quad (20)$$

Equation (19) determines an upper bound according to Voigt,[15] where strains are considered to be constant, to estimate Young's modulus of the composite by the rule of mixtures for stiffness components. Equation (20) determines a lower bound according to Reuss,[15] where stresses are considered to be constant in a composite, to estimate the Young's modulus by the rule of mixtures for compliance components. For the calculations of the upper and lower bounds of Young's modulus of $LaCoO_3$ as a function of applied stress, the following procedure was developed. Equation (17) was used for calculation of E_{hkl}, for the specific (hkl) directions using the elastic constants presented in Table III of this paper. These E_{hkl} values do not depend on the applied stress. Then, using Eq. (15), the f_{hkl} volume fraction of relevant domains with orientation of their (hkl) planes normal to the loading direction is calculated as a function of applied stress. The f_{hkl} values are stress dependent and will increase/decrease as a function of applied stress. After E_{hkl} and f_{hkl} are calculated, the upper and lower bounds of Young's modulus of $LaCoO_3$ are estimated using Eqs. (19) and (20), respectively. Therefore, stress independent elastic constants and stress dependent volume fraction of domains were employed for the calculation of the upper and lower bounds of Young's modulus.

III. RESULTS AND DISCUSSION

Examples of the diffraction patterns of $LaCoO_3$ collected at selected stress levels by detector 1 in the direction parallel to the stress axis and by detector 2 perpendicular to the stress axis are shown in Figs. 1(a) and 1(b). As already discussed in previous work,[7] the material was initially isotropic at the beginning of loading as confirmed by the identical diffraction patterns recorded by the two detectors. However, the formation of preferred orientation was quickly detected when loading started. The rhombohedral angle of

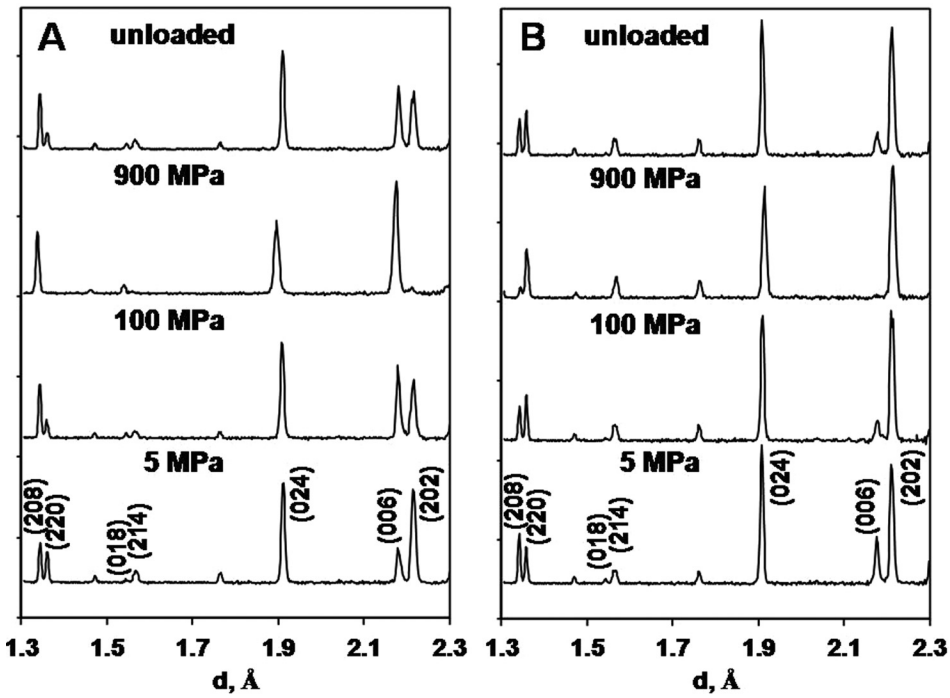

FIG. 1. Neutron diffraction patterns of polycrystalline $LaCoO_3$ collected at different stress levels (5, 100, and 900 MPa) during uniaxial compression and after removal stress. (a) Diffraction patterns collected by detector 1 in compression and (b) diffraction patterns collected by detector 2 in tension.

this material is 60.8°. The rhombohedral lattice constant is 5.37 Å. The evolution of the peak intensities depended on the Miller indices of the reflections and on the strain experienced by the lattice–compressive (detector 1) or tensile (detector 2). The (202) peak intensity decreased and the (006) peak intensity increased for detector 1 when the applied stress increased along the direction of detector D1. When the sample experienced tensile macroscopic strain in the direction perpendicular to the applied stress (D2), the (202) peak intensity increased and (006) peak vanished at high applied stress. Similar behavior was reported to occur in $La_{0.8}Ca_{0.2}CoO_3$ upon uniaxial compression.[11]

In the paper by Vullum *et al.*, the (*hkl*) peaks of $LaCoO_3$ were classified according to the orientation of the corresponding diffraction planes with respect to the *c*-axis and the reorientation of the domains was analyzed according to the angle between the loading direction and the *c*-axis of the domain. These angles for characteristic diffraction planes used for analysis in this paper are presented in Table II. In the case when the diffraction planes are perpendicular to the stress axis, the intensity of reflections increases with stress for diffraction planes with the angle between their normal and *c*-axis of less than 45°; while the intensity of reflections decreases with stress for diffraction planes with the angle between their normal and *c*-axis of higher than 45°. In the case when diffraction planes are parallel to the stress axis, the intensity of reflections increases for diffraction planes with the angle between their normal and *c*-axis higher than 45°, while the intensity decreases for diffraction planes with the angle between their normal and *c*-axis less than 45°. The reorientation of the domains increases the volume fraction of domains that have their *c*-axis more parallel to the stress axis. The volume fraction of domains with the angle between their *c*-axis and the loading direction of less than 45° increases at the expense of that of the domains with the angle between their *c*-axis and the loading direction higher than 45° due to domain reorientation.

The evolution of peaks' intensities and strain development in selected (*hkl*) reflections as a function of applied stress are shown in Fig. 2. The integrated peak intensities were measured as the area below the reflection, and are presented after normalizing the intensity with the initial intensity of each reflection at the beginning of loading. According to the orientation of the peaks relative to the *c*-axis, the intensities of the peaks can increase, decrease, or remain constant upon increase in applied stress. The intensities of

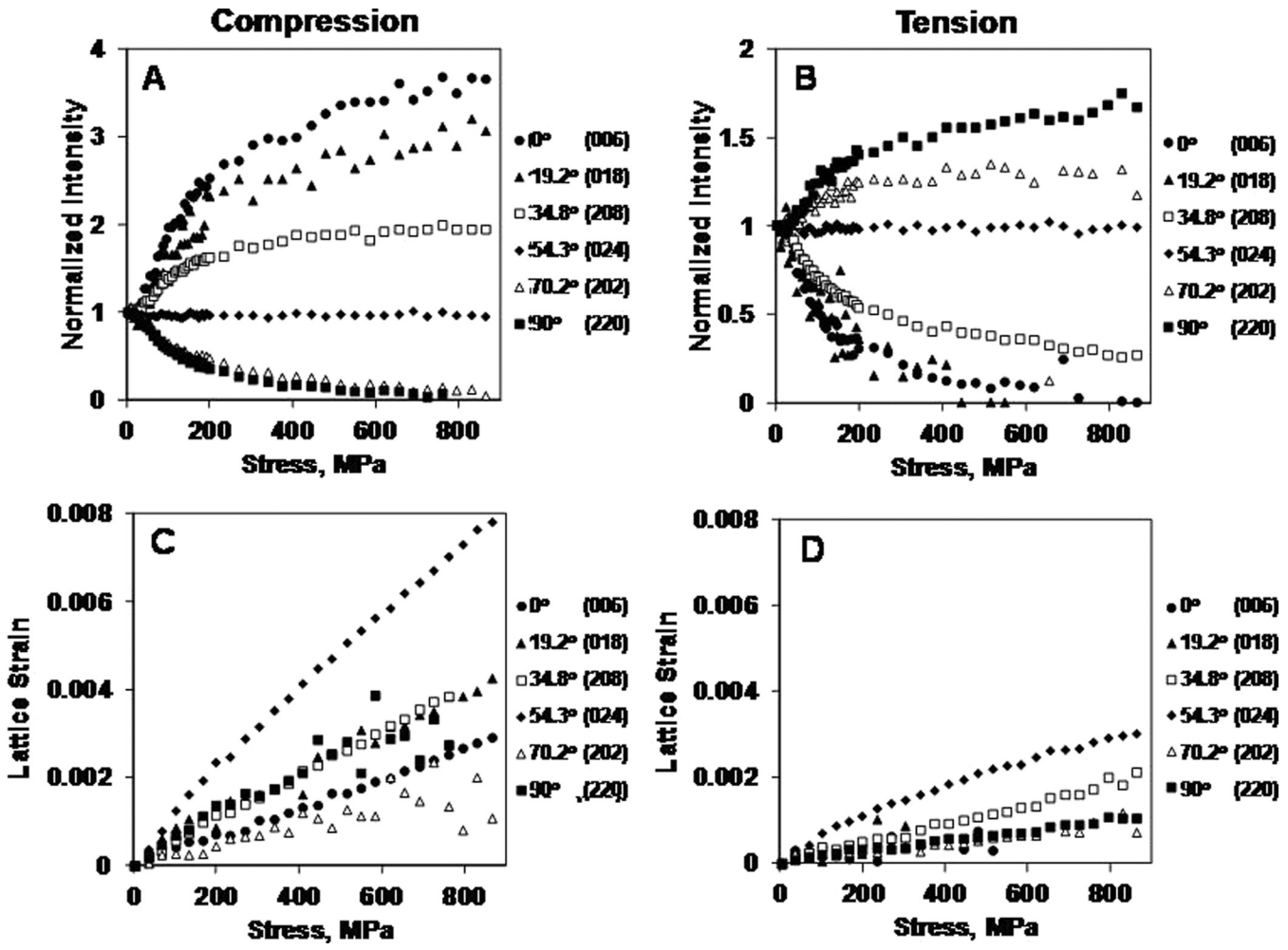

FIG. 2. (a) and (b) Intensities of (006), (018), (208), (024), (202), and (220) diffraction peaks normalized by the intensity of the corresponding peak at the beginning of the loading. (c) and (d) The calculated lattice strain for six selected peaks. (a) and (c) Data collected by detector 1; (b) and (d) data collected by detector 2.

the peaks collected by both detectors 1 and 2 are presented in Figs. 2(a) and 2(b). It is obvious from Fig. 2(a) that the intensities of the peaks from diffraction planes with the angle between their normal and *c*-ax of less than 45° grow under compression, while the intensities of peaks from diffraction planes with the angle between their normal and *c*-axis of more than 45° decrease, as was measured by detector 1. At the same time, the opposite changes in the intensities of the peaks are observed when planes exhibit tensile strains, as measured by detector 2. The intensity of the (024) peak remains constant and independent of applied stress both for compression and tension directions. The increase/decrease in the peaks' intensities indicates the increase/decrease in the volume fraction of mobile ferroelastic domains, due to domain movement and reorientation. The reorientation causes the increase in the volume fraction of domains that have their *c*-axis aligned more closely to the stress axis, such as the intensities of the peaks with high values of the Miller index *l* (and low *h* and *k*) increase, while the intensities of the reflections with high *h* and *k* values decrease. Exactly the same results are reported for $La_{0.8}Ca_{0.2}CoO_3$ and more description of the domain switching related to the $LaCoO_3$ based perovskites can be found in the work of Vullum *et al.*[11]

The individual $\varepsilon_{hkl}^{D1}(\sigma^{(i)})$ and $\varepsilon_{hkl}^{D2}(\sigma^{(i)})$ strains for six crystallographic planes under consideration calculated from the data obtained by detectors 1 and 2 are shown in Figs. 2(c) and 2(d). Five of the planes, (006), (018), (208), (202), and (220) belong to the doublets, whose intensities changed significantly depending on the orientation angle of the plane normal either parallel or perpendicular to the applied load, and one of the planes, (024), a singlet for which intensity did not change as applied load increased to 900 MPa. Each of the $\varepsilon_{hkl}^{D1}(\sigma^{(i)})$ and $\varepsilon_{hkl}^{D2}(\sigma^{(i)})$ strains represent the response of a family of domains oriented such that the given (hkl) lattice plane normal is parallel (Fig. 2(c)) and perpendicular (Fig. 2(d)) to the loading direction. The response of each individual plane under consideration deviates from linear behavior and does not represent a linear elastic response due to internal stresses, as one would expect the lattice to deform.

The authors do not treat the non-linear stress-strain response (Figs. 2(c) and 2(d)) as due to the presence of plastic deformation, but consider it as an effect of unknown internal stresses identified as local misfit stresses generated by the grain anisotropy. Lattice strain is treated as a linear function of total stress, which consists of a sum of the applied stress with a known value and a local internal stress with an unknown value. However, since the term is connected with internal stress, the strain shows a non-linear behavior as a function of applied stress. It is important to understand that an internal stress is not constant but is an unknown function of applied stress. Note that the domain wall motion can affect the accommodation of the internal stress.

The *hkl*-specific Young's moduli E_{hkl}, if calculated from the slopes of applied stress–lattice strain dependence, provide non-realistic values, such as $E_{006} = 250$ GPa, $E_{018} = 110$ GPa, $E_{208} = 180$ GPa, $E_{024} = 80$ GPa, $E_{202} = 300$ GPa, and $E_{220} = 140$ GPa, which are very different from the elastic modulus of isotropic polycrystalline $LaCoO_3$, which is 76 GPa as measured by an impulse excitation technique. They are not realistic because in addition to the applied stress $\sigma^{(i)}$, there is an additional local misfit stress σ_{hkl}^{m}, such that the stress $\sigma_{hkl}^{(i)}$ acting in each domain is a sum of the $\sigma^{(i)}$ and σ_{hkl}^{m} stresses. The local misfit stress σ_{hkl}^{m} is generated by the domain anisotropy and the misfit of the specific domain with the neighboring domains. This misfit stress can be more easily accommodated by the doublet planes which are mobile, easy to restructure and can participate in the domain switching, therefore, the resulting lattice strain calculated for (006)/(202), (208)/(220), and (018) planes is significantly lower, especially at high loads, in comparison with lattice strain which is calculated for the (024) plane. It indicates that the misfit stress will play a much stronger role in the deformation of crystallographic planes where no extra mechanisms of stress accommodations, such as domain switching, are present. The domain wall motion does not directly affect the value of Young's modulus. The domain wall motion can affect the accommodation of internal stress, with the internal stress affecting a non-linear dependence of strain as a function of applied stress. What is clear from calculations of the lattice strain of individual planes, is that the Young's modulus cannot be determined correctly using the data presented in Fig. 2(c), because the applied stress values do not correspond to the stress level located at each individual domain.

To calculate E_{hkl} and average lattice strains parallel and perpendicular to the loading direction, a_i^{D1}, c_i^{D1}, a_i^{D2}, and c_i^{D2} have to be determined. For these calculations, Eqs. (3) and (4) were utilized by averaging the *d* spacing data of six peaks using data collected from detectors 1 and 2 measurements. The results of the calculations are presented in Figs. 3(a) and 3(b). As one can see from Fig. 3, a decrease in a_i^{D1} and c_i^{D1} is observed when the planes are oriented perpendicular to the applied compressive stress, and when subjected to a tensile strain, an increase in the a_i^{D2} and c_i^{D2} lattice parameters is observed for the planes with parallel orientation toward applied stress direction. Once a_i^{D1}, c_i^{D1}, a_i^{D2}, and c_i^{D2} of $LaCoO_3$ were determined, $\varepsilon_{ave}^{D1}(\sigma^{(i)})$ and $\varepsilon_{ave}^{D2}(\sigma^{(i)})$ were also calculated (Fig. 3(c)). As already mentioned in Sec. II, $\varepsilon_{ave}^{D1}(\sigma^{(i)})$ coincides well with the continuum elastic strain measured by the extensometer during loading of the cobaltite, which is reported in previous work.[7] Therefore, it can be easily utilized for Young's modulus estimation of $LaCoO_3$ polycrystal as a function of applied stress. It is worth mentioning that while the average lattice strain versus applied stress data provides a small scatter of the experimental data points at lower stress levels, when the stress reaches 700–900 MPa, the scatter of the data becomes much more significant. A similar trend is also reported in the work of Daymond,[13] where the magnitude of the error in measuring of average elastic lattice strain was reported to be as high as 16% at high applied stress level. In this case, a larger scattering of the data is connected with a higher loading rate and broader stress interval for a given collection time (time interval to average neutron response) at higher stress levels.

As the average lattice strain was determined for planes under compressive and tensile deformations, as measured by detectors 1 and 2, this would give us a chance to determine Poisson's ratio ν by dividing the lateral strain $\varepsilon_{ave}^{D2}(\sigma^{(i)})$ by the

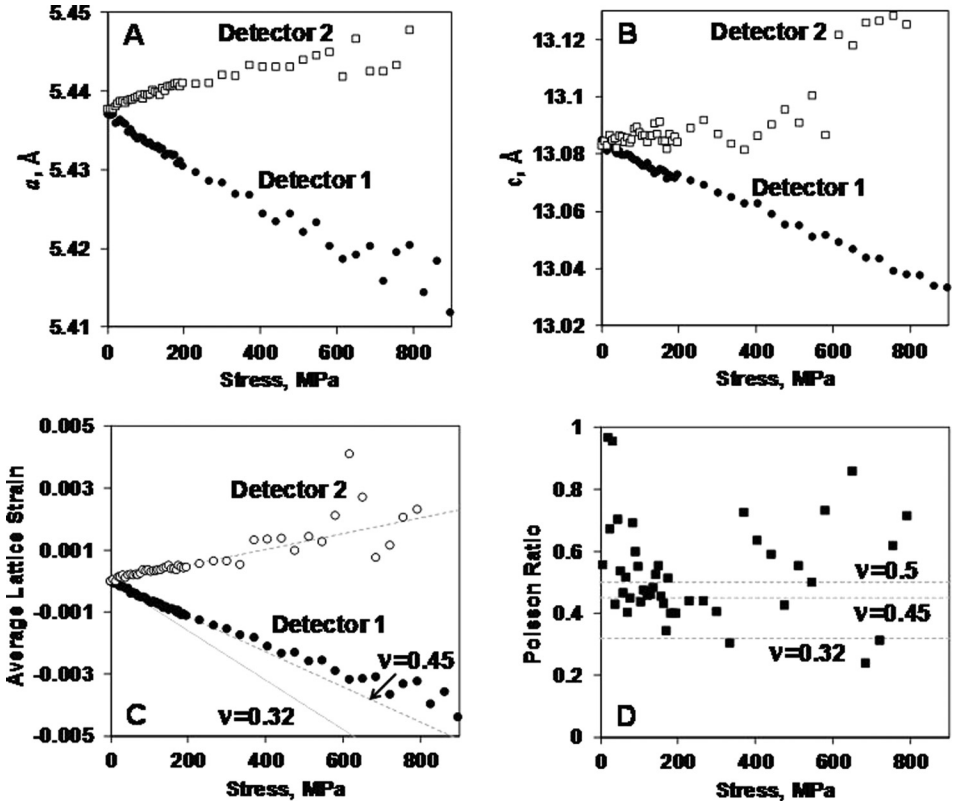

FIG. 3. The a_i^{D1} and a_i^{D2} (a) and the c_i^{D1} and c_i^{D2} (b) lattice parameters of $LaCoO_3$ presented as a function of applied stress. (c) The average lattice strain, calculated using the a_i^{D1}, c_i^{D1}, a_i^{D2}, and c_i^{D2} lattice parameters as a function of applied stress. The best fit lines are also shown to indicate the average radial and lateral strain values used for calculation of Poisson's ratio. In addition, radial strain value which can correspond to the measured Poisson's ratio by impulse excitation technique is also shown for clarity. (d) Poisson's ratio as a function of applied stress.

axial strain $\varepsilon_{ave}^{D1}(\sigma^{(i)})$. If we directly use the experimental strain values, as presented in Fig. 3(c) to calculate ν, a very large scattering of the experimental Poisson's ratio data points occurs (Fig. 3(d)). If we fit $\varepsilon_{ave}^{D1}(\sigma^{(i)})$ and $\varepsilon_{ave}^{D2}(\sigma^{(i)})$ with straight lines, then the ratio of the slopes of these lines provides us with a Poisson's ratio ν value equal to 0.45. Note that using $\varepsilon_a^{D1}(\sigma^{(i)})$ and $\varepsilon_a^{D2}(\sigma^{(i)})$, we obtain Poisson's ratio equal to 0.5, and using $\varepsilon_c^{D1}(\sigma^{(i)})$ and $\varepsilon_c^{D2}(\sigma^{(i)})$, we have $\nu = 0.32$. The experimentally measured value of $LaCoO_3$ Poisson's ratio by impulse excitation technique is equal to 0.32. The fitting straight line for $\varepsilon_{ave}^{D1}(\sigma^{(i)})$ with the slope corresponding to ratio 0.32 is also shown in Fig. 3(c), along with the values of Poisson's ratio calculated using $\varepsilon_a^{D1}(\sigma^{(i)})$, $\varepsilon_a^{D2}(\sigma^{(i)})$ and $\varepsilon_c^{D1}(\sigma^{(i)})$, $\varepsilon_c^{D2}(\sigma^{(i)})$. The ultimate $\nu = 0.5$, the ratio 0.45, and Poisson's ratio 0.32 measured by acoustic technique are shown in Fig. 3(d). The acoustic technique allows the measurement of Young modulus E and the shear modulus G with Poisson's ratio calculated as $E/2G - 1$. Since it is not known if Poisson's ratio would change as the applied stress increases, it might be that the obtained values are valid only at the beginning of loading, where the applied stress is small and the material is isotropic. The value of Poisson's ratio of 0.45 presented is quite large indeed. Inelastic deformation (non-linearity of strain-stress dependence), low accuracy of lattice strain determination, effect of internal stresses can all contribute to the high value reported. Therefore, more research is required to clarify the dependence of Poisson's ratio of $LaCoO_3$ on applied compressive stress.

For pure hexagonal structure, there are five non-zero compliance coefficients. While the $R\bar{3}c$ rhombohedral structure of $LaCoO_3$ can be described using a hexagonal unit cell, strictly speaking it does not possess hexagonal symmetry since it does not have a six-fold symmetry and only a three-fold rotational symmetry about the c-axis. Therefore, for $R\bar{3}c$ rhombohedral structures, six non-zero compliance coefficients exist, but in order to determine E_{hkl}, one needs to know only five of them. If we know the compliance coefficients S_{11}, S_{33}, S_{44}, S_{13}, S_{14}, and a_i^{D1} and c_i^{D1} lattice parameters, we can easily determine the Young's modulus of the compounds in a specific crystallographic direction, which is perpendicular to the (hkl) plane of interest. The values of five compliance coefficients have been estimated using Eqs. (17) and (18) (Table III). Fig. 4(a) shows the calculated values of E_{hkl} as a function of angle between plane normal and the c-axis of the lattice. The solid line, also presented in Fig. 4(a), is given for guidance and corresponds to the theoretical dependence of Young's modulus versus plane orientation angle for six-fold hexagonal structure. As one can see, there is perfect agreement between three-fold $LaCoO_3$ and six-fold hexagonal lattice for the planes with 0° and 90° angle, as is predicted by theory. However, the discrepancies between the two structures exists for (018), (208), (024), and (202) planes, since to elastically characterize the linear elastic properties of $R\bar{3}c$ rhombohedral structure, more non-zero compliance coefficients are needed compared to the hexagonal structure. As one can see from Fig. 4(a), the directions perpendicular to (006), (018), and (208) planes have higher elastic moduli in comparison with directions perpendicular to the (024), (202), and (220) planes. The volume fraction of (006), (018), and (208) domains increases when a uniaxial compressive stress is applied. From macroscopic stress-strain deformation plots, one can see that the Young's modulus of the $LaCoO_3$ polycrystal increased significantly when the stress was high, such as 900 MPa[7] and severe texture in $LaCoO_3$ is present. Such an increase in the Young's modulus of the polycrystalline material can be easily explained by the

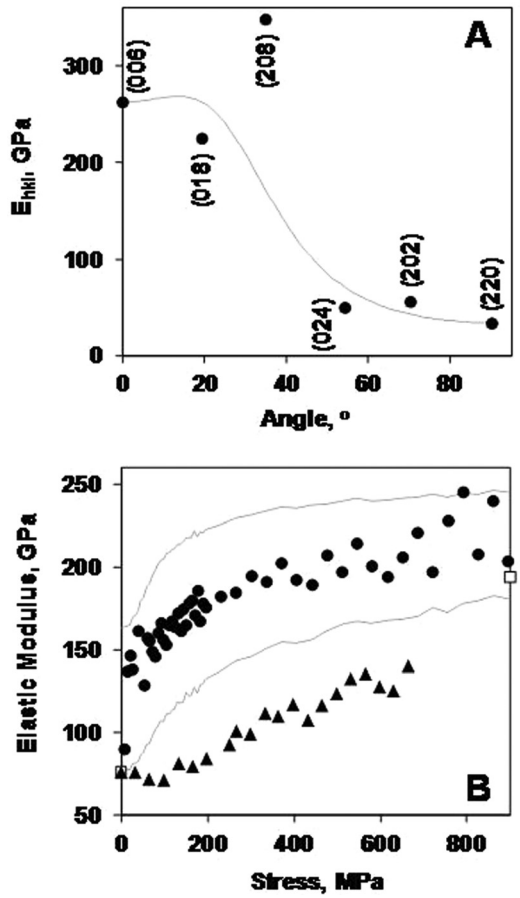

FIG. 4. Calculated Young modulus for different crystallographic directions (solid line is the dependence for pure hexagonal lattice for comparison) (a) and corresponding estimated upper and lower boundaries (solid lines) for Young's modulus of polycrystal (b). Circles are the elastic modulus values measured utilizing average lattice strain. Squares are the elastic modulus values calculated as a slope of the macroscopic stress-strain deformation curve measured by the extensometer during neutron diffraction experiments. Triangles are the elastic modulus values measured in cyclic compression experiments where the incremental increase in load was applied.

increase in the volume fraction of single domains with high Young's moduli along the loading direction.

Since $\varepsilon_{ave}^{D1}(\sigma^{(i)})$ corresponds well to macroscopic elastic strain, Young's modulus as a function of applied stress for $LaCoO_3$ can be determined utilizing Eq. (12). The results of such calculations are presented in Fig. 4(b) as circles. As one can see from Fig. 4(b), a rather significant increase in Young's modulus is reported when the applied stress increases from about 5 MPa at the beginning of the loading to the maximum compressive stress of 900 MPa. The Young's modulus value measured at the beginning of loading, where the material is still isotropic is shown in Fig. 1, corresponds well with the values measured both by impulse excitation technique and from the slope of the macroscopic stress-strain deformation curve published in previous work.[7] The results shown in Fig. 4(b) at zero applied stress provide the Young's modulus value equal to 76 GPa, as it was reported in earlier publications.[5,7] As the texture and domain reorientation developed very fast at small applied stress,[7] the fast increase in the Young's modulus to ~145–150 GPa at small applied stress (30–50 MPa) can be seen in Fig. 4(b). As the $\sigma^{(i)}$ values grow to the maximum compressive stress (900 MPa), an increase in the Young's modulus is further observed. For comparison, the value of Young's modulus calculated as a slope of the macroscopic stress-strain deformation curve measured by the extensometer during neutron diffraction experiments at 900 MPa while unloading began is also presented in Fig. 4(b) as squares. It is important to notice here that excellent agreement was found not only for Young's modulus values obtained from the extensometer and average lattice strain measurements, but it is also equal to the measured portion of macroscopic elastic strain, equal to 0.0046 at 900 MPa, from the macroscopic stress-strain curve and the calculated value of average lattice strain $\varepsilon_{ave}^{D1}(\sigma^{(i)})$, equal to 0.0044 at the same applied stress, which shows an excellent coincidence too. For estimation of the upper and lower bounds of the Young's modulus of polycrystalline $LaCoO_3$, the compliance coefficients presented in Table III along with the intensities of (*hkl*) peaks reported in previous work[7] were used. The Eqs. (19) and (20) were employed in these calculations. As one can see, there is a perfect match between predicted upper and lower bounds and the elastic modulus values measured utilizing average lattice strain $\varepsilon_{ave}^{D1}(\sigma^{(i)})$ as well as two experimental data points obtained at the beginning of loading and 900 MPa applied stress from the macroscopic measurements. Such good coincidence of the experimental and calculated results verify the validity of the compliance coefficients and significant elastic anisotropy of the $LaCoO_3$ ceramic formed during uniaxially compressed samples.

For further independent verification of the formation of elastic anisotropy, several $LaCoO_3$ samples have been uniaxially compressed where the incremental increase in load was applied during cycling and no neutron diffraction was performed during compression. It was found that Young's modulus of such samples was equal to 76 GPa at the beginning of loading, which is the same value as it was measured for other isotropic $LaCoO_3$ ceramics. However, instead of showing a rather sharp increase in elastic modulus at small 30–50 MPa loads as it is seen for the sample under neutron irradiation, the Young's modulus remains almost constant or slightly decreases as the applied stress increased to 130 MPa, and the Young's modulus slowly increases its values as the applied stress increased further. At a high applied stress (700 MPa), the Young's modulus was measured to be equal to 140 GPa which is significantly lower than the values measured during neutron diffraction experiments. While there is a clear difference between material behaviour when neutron radiation is present or absent, the reason for such discrepancies is not well understood. At least two factors can contribute: first factor is radiation effect on the domain walls' movement and texture formation, and the second factor is different loading rates used in the experimental procedure. It is fair to expect that bombardment of $LaCoO_3$ by neutrons may produce defects, as it was reported for SiC or B_4C and many other ceramics, and alleviate domain movement making domain boundaries much more mobile and texture more easy to form. However, the energies of thermal neutrons used in the current experiment at SNS are fairly low (<400 meV), comparable with those of phonons, thus it is not likely that such significant differences in the domain

walls' mobilities and stiffening of the $LaCoO_3$ would be caused by the neutron radiation. At the same time, the loading rate of the $LaCoO_3$ sample during neutron diffraction experiments was equal 1.3 MPa/min which was more than 100 times slower in comparison with 180 MPa/min used for separate cyclic uniaxial compression where no neutrons were present. This material exhibits time dependent mechanical behavior, i.e., it is rate sensitive. As there was more time allowed for domains switching in the latter, this also might contribute to the formation of stronger elastic anisotropy at lower applied stresses, causing the discrepancies between the experimental results.

An assumption is made that the initial state of $LaCoO_3$ is isotropic as it is a polycrystalline material, therefore no texture is present. The isotropic material shows a certain value of Young's modulus. After loading, texture develops which affects the modulus values. Therefore comparison of these values is of importance for better understanding of the material's behavior. The elastic modulus measured by excitation technique corresponds to the initial state of the material before loading (without texture). The loading modulus (from neutron diffraction data) in Fig. 4 is a theoretical estimation of elastic modulus in the compression direction where a corresponding texture is taken into account at different applied stresses. The unloading modulus is an experimental value of the elastic modulus of $LaCoO_3$ in the compression direction corresponding to certain applied stress and formed texture. This value was measured at the beginning of unloading and, in fact, corresponded to the Young's modulus of the textured material obtained during loading up to a certain stress value. This way, the different values of Young's modulus can be compared.

IV. CONCLUSIONS

Elastic anisotropy in originally isotropic polycrystalline $LaCoO_3$ perovskite during the uniaxial compression has been studied. The texture formation and preferred domain orientation have been investigated. The lattice strains of individual (*hkl*) planes as well as average lattice strain were determined both for the planes oriented perpendicular and parallel to the loading direction. Utilizing average lattice strains as well as lattice strains along a and c crystallographic directions, an attempt was made to determine the Poisson's ratio, which was then compared with the Poisson's ratio value measured by impulse excitation technique. The elastic constants were calculated and Young's moduli of $LaCoO_3$ single crystal in different crystallographic directions were estimated. The verification of the obtained results was performed by estimation of the upper and lower bounds of elastic modulus of polycrystalline material as a function of applied compressive stress, which showed an excellent coincidence with Young's modulus values calculated from average lattice strain and macroscopic stress-strain deformation plot of sample used in neutron diffraction experiment. The question remains if neutron radiation or loading rates affect the elastic anisotropy of the material during uniaxial compression.

ACKNOWLEDGMENTS

This work was supported by the NSF Project No. CMMI-0968911 "Time Dependent Creep Deformation of Non Polar Mixed Conducting Ferroelastic Perovskites". Research conducted at ORNL's Spallation Neutron Source (SNS) was sponsored by the Scientific User Facilities Division, Office of Basic Energy Sciences, U.S. Department of Energy.

[1]N. Orlovskaya, Y. Gogotsi, M. Reece, B. Cheng, and I. Gibson, Acta Mater. **50**, 715 (2002).
[2]N. Orlovskaya, N. Browning, and A. Nicholls, Acta Mater. **51**, 5063 (2003).
[3]M. Lugovy, V. Slyunyayev, N. Orlovskaya, D. Verbylo, and M. Reece, Phys. Rev. B **78**, 024107 (2008).
[4]S. Faaland, T. Grande, M. A. Einarsrud, P. E. Vullum, and R. Holmestad, J. Am. Ceram. Soc. **88**, 726 (2005).
[5]N. Orlovskaya, M. Lugovy, S. Pathak, D. Steinmetz, J. Lloyd, L. Fegely, M. Radovic, E. A. Payzant, E. Lara-Curzio, L. Allard, and J. Kuebler, J. Power Sources **182**, 230 (2008).
[6]J.-S. Zhou, J.-Q. Yan, and J. B. Goodenough, Phys. Rev. B **71**, 220103(R) (2005).
[7]A. Aman, Y. Chen, M. Lugovy, N. Orlovskaya, M. J. Reece, D. Ma, A. Stoica, and K. An, J. Appl. Phys. **116**, 013503 (2014).
[8]S. Pathak, J. Kuebler, E. A. Payzant, and N. Orlovskaya, J. Power Sources **195**, 3612 (2010).
[9]M. Lugovy, N. Orlovskaya, and M. Reece, "Uniaxial compression of $LaCoO_3$" (unpublished).
[10]EN 843-2:2006, "Advanced technical ceramics. Mechanical properties of monolithic ceramics at room temperature. Determination of Young's modulus, shear modulus and Poisson's ratio."
[11]P. E. Vullum, J. Mastin, J. Wright, M.-A. Einarsrud, R. Holmestad, and T. Grande, Acta Mater. **54**, 2615 (2006).
[12]M. R. Daymond, M. A. M. Bourke, and R. B. Von Dreele, J. Appl. Phys. **85**, 739 (1999).
[13]M. R. Daymond, J. Appl. Phys. **96**, 4263 (2004).
[14]I. Sirotin Yu and M. P. Shaskolskaya, *Fundamentals of Crystal Physics* (Mir Publishers, Moscow, 1982).
[15]W. D. Callister, Jr., *Materials Science and Engineering: An Introduction*, 7th ed. (John Wiley & Sons, Inc., 2007), p. 750.